ELSEVIER

Journal of Hazardous Materials B80 (2000) 207–221

Journal of Hazardous Materials

www.elsevier.nl/locate/jhazmat

Synthesis and characterization of catalysts produced from paper mill sludge I. Determination of NO_x removal capability

Nasrin R. Khalili*, Hitendra Jain, Hamid Arastoopour

Department of Chemical and Environmental Engineering, Illinois Institute of Technology, 10 W. 33rd Street, Chicago, IL 60616, USA

Received 10 March 2000; received in revised form 2 August 2000; accepted 2 August 2000

Abstract

Characteristics and catalytic properties of a series of carbon-based catalysts (CBCs) produced from paper mill sludge were evaluated. The major processes involved in the production of the catalysts were chemical activation, impregnation, pyrolysis, and post pyrolysis rinsing. The porous structure, catalytic activity and thermostability of the catalysts were tailored during the production stage by introducing hetero-atoms (zinc chloride, and ferric nitrate) in the carbon structure. Characterization of the produced CBCs included determination of the surface area, pore size, and pore size distribution (PSD) from standard N_2-adsorption isotherm data. The extent of graphitization and the presence of metal crystals were identified from X-ray diffraction (XRD). The limit of the catalyst gasification was estimated from thermogravimetric analysis (TGA) conducted in an oxidized environment. The NO_x reduction capability of the produced catalysts was evaluated in the presence of carbon monoxide using a fixed bed reactor. The reaction temperature ranged from 300 to 500°C. It was shown that paper mill sludge is an excellent precursor for the production of CBCs with NO_x removal capability of 66–94%. The catalytic capability of the produced CBCs varied according to the method of production, catalyst surface properties (surface area, pore structure, PSD), metal composition and reaction temperature. The highest NO_x removal capacity was observed for the catalytic reactions carried out at 400°C. The mesoporous catalyst produced with a Zn:Fe molar ratio of 1:0.5 exhibited the maximum NO_x removal catalytic activity of 94%.

Keywords: Carbon-based catalysts; Paper mill sludge; NO_x removal; Catalytic activity

* Corresponding author. Tel.: +1-312-567-3534; fax: +1-312-567-8874.
E-mail address: khalili@iit.edu (N.R. Khalili).

0304-3894/00/$ – see front matter
PII: S0304-3894(00)00304-6

1. Introduction

The issue of air pollution has continued to be the subject of regulatory activity, particularly in the United States. The passage of the 1990 Clean Air Act Amendment has addressed the entire range of air pollutants, particularly emission of oxides of nitrogen (NO_x). Initially, combustion modification techniques were considered to reduce the amount of NO_x formed during combustion processes. However, the usefulness of this process was questioned when it was shown that combustion modifications reduce boiler efficiency, and increase soot formation, and CO and particulate loading in the flue gas [1]. Stringent NO_x emission regulations have forced industry to develop flue gas treatment (FGT) strategies which use catalytic reduction processes such as selective non-catalytic reduction (SNCR), non-selective catalytic reduction (NSCR) and selective catalytic reduction (SCR). Among these processes, the SCR has shown promising results for effective reduction of NO_x to N_2 at temperatures above and near 350°C [1–3].

The SCR process commonly uses reductant gases such as ammonia (NH_3). The usage of this gas is, however, becoming limited due to the problems detected with slippage of NH_3 or other reductants and production of unwanted side reaction products such as HCN [1,2,4]. Other reducing agents used for SCR systems are carbon monoxide (CO), hydrogen, methane and some hydrocarbons. Tremendous attention is given to the application of CO since this gas is also a major air pollutant, its usage widens the reaction temperature window, and when used at low concentration, it provides a sufficiently reduced environment to significantly enhance the NO_x catalytic removal efficiency at any given temperature [1,5–7].

The effectiveness of the SCR process is controlled by the reaction temperature, catalyst metal composition and the reaction condition. Since a catalyst participating in NO_x reduction reactions must be capable of giving an electron to nitric oxide, and possibly accepting an electron from the other reactant/products for cleaning, breaking the N–O bond [8,9], the temperature range of the NO–CO reaction has a strong influence on the catalyst activity [5,6]. Structural properties of the catalyst, i.e. distribution characteristics of the salt, can also have a significant impact on the effectiveness of the SCR system. The presence of inhibiting components such as oxygen during the catalytic reduction reaction must also be minimized in order to obtain maximum efficiency in SCR systems [2].

The SCR process commonly utilizes catalysts consisting of a variety of metal oxides such as vanadium, chromium, titanium, rhodium, palladium, and copper supported on inert material such as activated carbons, silica, alumina, and molecular sieves. Recently, it was shown that the use of a particular carbon support, together with metal clusters serving as catalyst precursors, allows the achievement of high metal dispersions and production of catalysts with improved catalytic properties [2,9–11].

Among a variety of catalysts studied, activated carbon-based catalysts (CBCs) containing metal oxides (copper or iron oxides) have been shown to be very active for NO_x reduction because of their high surface area and ability to catalyze the NO_x reduction reaction at low temperature [9,12,13]. However, the use of expensive noble metals for the production of the catalysts and the gradual loss of these metals during the regeneration process has affected the economic viability of these catalysts [7,11].

The solutions provided to the cost-related problems of the SCR systems include replacement of the commercially available noble catalysts with cost effective catalytic materials

that can effectively reduce NO_x at a low temperature; substitution of the expensive noble metals with less expensive metal oxides such as iron salts; and further, replacement of the commercially available activated carbon support with other high surface area, low cost activated carbons such as those produced from carbonaceous waste material [5,9,14–16]. These carbons have found extensive application in the treatment of wastewater polluted with large toxic molecules, hydrogen sulfide removal, NO_x and phosphine abatement, and decomposition of peroxide [17,18].

This paper presents the results of a study conducted to (a) evaluate the feasibility of using paper mill sludge for the production of cost-effective CBCs, and (b) examine NO_x removal activity of the produced catalysts. Paper mill sludge was selected because of its carbonaceous properties, mass production, and the negative cost affiliated with the economic burden of its production and disposal.

The process focused on the production of catalysts with high NO_x reduction capability. Catalytic activity was enhanced by promoting the outgrowth of chemically active centers from carbonaceous material that served as a precursor (sludge), and metal salts (zinc chloride and iron nitrate) that were used as impregnating agents. Zinc chloride was used to enhance pore structure development [16–19] and iron salt provided a precursor for the augmentation of the catalytic NO_x reduction reactions [2,6,21].

2. Experimental procedure

2.1. Production of CBCs

A number of unit operations and unit processes were involved in the production of CBCs from paper mill sludge. The initial chemical analysis of the sludge indicated 34% C, 5.2% H, 0.24% S, and drying loss of 3.7%.

The selected unit processes were primarily responsible for the composition, characteristics and the catalytic properties of the produced catalysts. Initially, two different strategies were considered for the catalyst preparation: impregnation during the synthesis of the carbon or impregnation upon production of the activated carbon. Method 1 was used assuming that impregnating with salt (zinc chloride and iron nitrate) during chemical activation rather than after production would avoid the blockage of the pores and provide more uniform distribution of the active sites on the carbon surface [2].

To produce the catalysts, paper mill sludge was initially dried, crushed, and sieved prior to chemical impregnation. During chemical impregnation, the weight ratio of the dried sludge to that of the impregnating agents was kept constant (about 25%); however, the impregnating agents ratios, namely, zinc chloride to iron nitrate, were varied to evaluate the impact of iron concentration on catalytic properties of the produced CBCs. Upon completing chemical impregnation, which was carried out for 7 h at 80°C, samples were dried in an oven at 110°C for 24–36 h. After drying, samples were crushed into fine powder and were later exposed to the atmosphere for 22 h at room temperature, as was suggested by Khalili et al. [16]. Pyrolysis of the samples was conducted at 750°C for 2 h in an inert environment (presence of N_2 gas). Upon completion of the pyrolysis, the produced catalysts were removed from the reactor and crushed using a mortar and pestle. Except for $[C\text{-}ZnFe]_{1,a}$, all of the catalysts

were rinsed with 1 M solution of hydrochloric acid and water, then dried and stored in a closed container for further analysis.

2.2. Surface characterization

2.2.1. Determination of the surface chemical and physical properties

The chemical analysis indicated that CBCs on average contain 46% C, 2% H, 0.75% N_2, 0.49% S, and 38% ash. The C:H ratio was 6.5:22.4% for the raw material and the produced CBCs. Depending on the method of production, the Zn and Fe weight percent in the produced CBCs varied from 0.2 to 4.6% and 0.0 to 1.2%, respectively.

The surface area, extent of the micro- and mesoporosity, and pore size distribution (PSD) were evaluated from the Brunauer, Emmet and Teller (BET) model applied to the N_2-adsorption isotherm data. It was assumed that the surface area, A, is related to the monolayer capacity by the simple equation $A = n_m a_m L$, where a_m is the average area occupied by a molecule of the adsorbate in the completed monolayer and L the Avogadro constant, taking 0.162 nm^2 as the cross-sectional area of a nitrogen molecule [22].

2.2.2. X-ray diffraction

X-ray diffraction (XRD) was used to determine the types of crystal structures present in the primary matrix of the catalysts. Diffraction of the X-rays through the sample provided some qualitative data about the presence or absence of graphite-like structures as well as metal salt crystals in the products. The analysis of X-ray diffraction relied on application of the Bragg law ($n\lambda = 2d \sin\theta$), where n is an integer, generally 1, λ the wavelength of the X-radiation (in Å), d the interplanar spacing (in Å), and θ the Bragg angle, or the angle that defines the spacing between atoms in a crystalline structure [20,23].

2.2.3. Catalytic activity measurements

Preliminary fly ash extruded with alumina, an active catalyst for NO_x removal (unpublished data) was used to test the proper functioning of the instruments used for the catalytic studies. The experimental set-up (Fig. 1) consisted of a quartz reactor that had dimensions of 6.3 mm internal diameter and 52 mm height. The reactor was equipped with a mesh screen for supporting the catalyst. The reactor was placed in a furnace equipped with a temperature-programming unit. The flow rate of the gas entering the reactor was measured using a flow meter. The fluidization and channeling effects were minimized by proper manipulation of the flow and gas distribution. A cyclone separator placed at the outlet of the reactor prevented any particulate from reaching the measuring instrument (NO/NO_x analyzer). A Chemiluminescent NO_x analyzer was used to measure the concentration (in ppm) of the gases (NO/NO_2) exiting the reactor.

To evaluate the impact of the temperature and flow direction on the catalytic capability, the produced CBCs and fly ash extruded with alumina (control catalyst used in this study) were exposed to an NO_x inlet concentration of 1000 ppm (nitric oxide and N_2) and flow rate of 90 ml/min. If not stated otherwise, carbon monoxide was used as a reducing agent. Catalysts were pre-treated with N_2 at 50°C/min to 400°C for 30 min prior to the catalysis study (pre-treatment of the catalyst in N_2 gas at a temperature of 400°C, significantly improved the breakthrough time of the catalytic reaction).

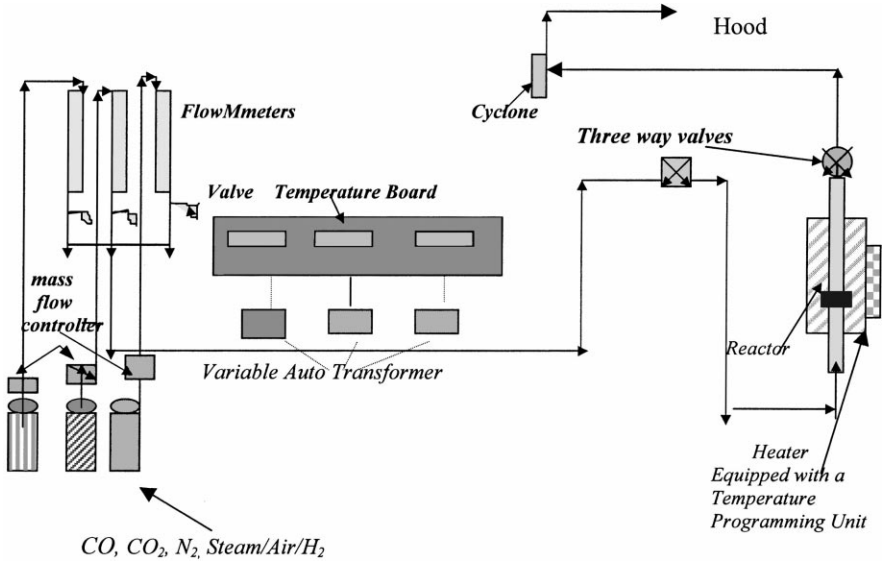

Fig. 1. Experimental set-up.

Thermogravimetric analysis (TGA) was conducted to predict the activation energy associated with the gasification ability of the produced catalysts in oxidized environments. The observed activation energy and catalytic activities of the catalysts were correlated with the method of production (impregnation ratio, post pyrolysis rinsing), surface properties and processing conditions.

3. Results and discussion

3.1. Analysis of the surface physical properties

The famous BET model (Eq. (1)) was used to evaluate the catalyst surface area, a primary measure of adsorption and catalytic activity. The BET model assumes that the surface of an adsorbent (CBC in this study) is completely covered by an adsorbate monolayer, and that the monolayer coverage can be calculated if the molecular dimensions of the adsorbate and the amount adsorbed are known [22,24]

$$\frac{p/p_0}{V(1-p/p_0)} = \frac{1}{V_m c} + \frac{c-1}{V_m c}\left(\frac{p}{p_0}\right) \tag{1}$$

The important parameters in this model are: p the equilibrium partial pressure, p_0 the saturation vapor pressure, V the volume adsorbed, V_m the monolayer capacity and c the dimensionless constant from which net heat of adsorption can be calculated.

The N_2 adsorption isotherms obtained for the produced CBCs are shown in Fig. 2. The adsorption data were used to estimate the monolayer volume, constant c, and the net heat

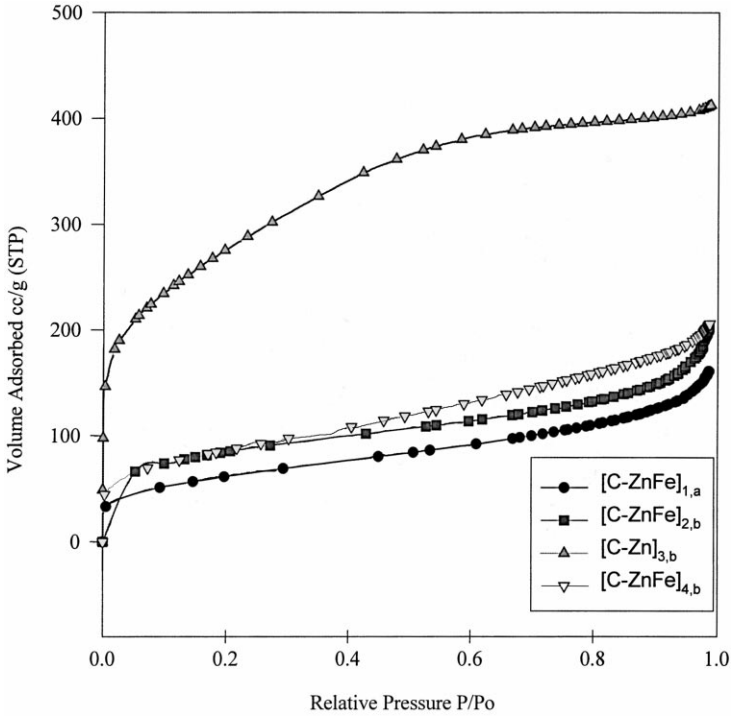

Fig. 2. Nitrogen adsorption isotherms of produced CBCs.

of adsorption, $q_1 - q_L$. The BET total surface area, micro- and mesopore surface areas, monolayer adsorption capacity and the net heat of adsorption obtained for the CBCs are presented in Table 1. This table shows that an increase in the amount of iron salt used during impregnation results in a decrease in the surface area and monolayer volume, V_m. The estimated surface area and the level of micro- and mesoporosity varies according to the employed method of production, i.e. the amount of chemicals used during chemical impregnation processes. The lowest surface area and lowest heat of adsorption were observed for the $[C\text{-}ZnFe]_{1,a}$ (the catalyst produced without post pyrolysis rinsing) and was related to the presence of impurities, pore clogging, and improper distribution of the metals on the surface of this catalyst [25].

The total catalyst surface area varied between 224 and 996 m^2/g. The highest surface area and most microporous structure were observed for the catalyst produced in the absence of iron salts, $[C\text{-}Zn]_{3,b}$. The BET total surface area and mesoporosity of the catalyst $[C\text{-}ZnFe]_{4,b}$ was higher than that of the catalyst $[C\text{-}ZnFe]_{2,b}$. As shown in Table 1, the amount of Zn:Fe used at the impregnation stage has a profound impact on the surface characteristics of the produced catalysts.

Since the characteristic of the PSD can significantly impact the extent of gas–solid diffusion resistance and the interaction of the gaseous reactants (CO + NO) on the walls or the surface of the catalyst [4,10,18,22], the systematic development of micro- and mesopores

Table 1
Surface area and micropore volume of the catalyst series

CBCs	Zn:Fe molar ratio	BET surface area (m^2/g)	Micropore surface area (m^2/g)	Mesopore surface area (m^2/g)	Net heat of adsorption ($q_1 - q_L$)[a] (kcal/mol)	V_m[b], (STP) (ml/g)
$[C\text{-}ZnFe]_{1,a}$[c]	1:1	224	19.1	205	0.689	51.5
$[C\text{-}ZnFe]_{2,b}$[d]	1:1	302	77.6	226	0.813	69.4
$[C\text{-}Zn]_{3,b}$[e]	No iron	996	113	883	0.731	229
$[C\text{-}ZnFe]_{4,b}$	1:0.5	310	39.2	271	0.737	71.3

[a] $q_1 - q_L = RT \ln c$ (R the universal gas constant, T the adsorption temperature (77 K)).

[b] V_m calculated from $A = (V_m/22414)a_m L \times 10^{-20}$, where a_m represented the average area occupied by a molecule of adsorbate in the completed monolayer, L the Avogadro constant, and a_m was calculated from the molecular weight and the density of the adsorbing gas (N_2) ($a_m = 1.091(M/\rho_L L) = 16.2\,Å^2$, where $M = 28$ g/gmol and $\rho_L = 0.81$ g/cm^3).

[c] Catalysts produced without post pyrolysis rinsing with HCl and H_2O.

[d] Catalysts produced with post pyrolysis rinsing.

[e] Sample with zero iron.

in the structure of the produced CBCs was evaluated and expressed in terms of PSD. Fig. 3 demonstrates the effect of the method of production on the extent and the uniformity of the PSDs. As shown, a very distinct difference was observed between the pore sizes. The catalyst $[C\text{-}Zn]_{3,b}$ has a high surface area but nonuniform PSD (approximately 70% of the pores are in the size range of 0–6 nm). A well-defined PSD is, however, observed for the catalysts containing iron in their structure. The most uniform PSD is observed for the catalyst $[C\text{-}ZnFe]_{4,b}$ that was prepared with a Zn:Fe molar ratio of 1:0.5. As shown in Table 1, this catalyst also has a more distinguished mesoporous structure.

These observations suggested that characteristics and the amount of chemicals used during impregnation could significantly impact the surface properties of the produced catalysts.

3.2. X-ray diffraction

XRD patterns provided useful information about the types of crystal systems and presence or absence of graphite-like structures in the primary matrix of the produced catalysts. By using X-rays of known wavelength λ and measuring θ (2θ is the angle between the diffracted beam and the transmitted beam, known as the diffraction angle), plane spacing d in the crystal was determined using Eq. (2) [20,23]. The d values identified the type of crystals present in the produced CBCs.

$$d = \frac{\lambda}{2 \sin \theta} \tag{2}$$

Fig. 4 shows the XRD plots and estimated plane spacing, d (Å), for the dominant peaks. The peaks at $d \sim 3.4$ Å ($2\theta = 26$) were identified as the reflection of graphite-like structure, while the peaks at $d = 2.01$, 2.4, 2.8 and 2.9 Å were attributed to the $ZnCl_2$ crystals. The other peaks were related to the presence of $Fe_3(NO_3)_2$ crystal which was identified in the catalyst $[C\text{-}ZnFe]_{4,b}$ at $d = 1.8$ Å.

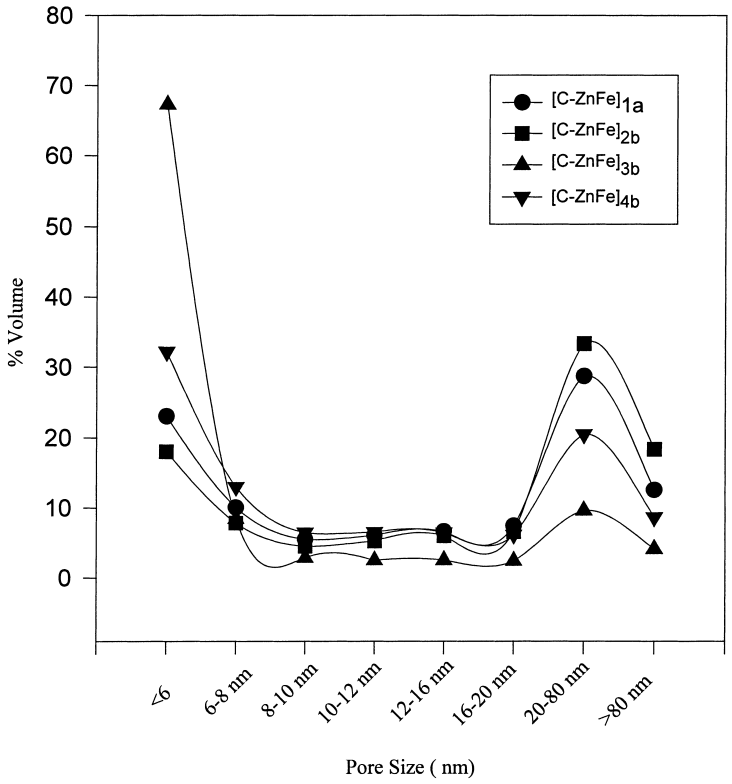

Fig. 3. Pore size distribution of the produced CBCs from paper mill sludge.

The presence of graphite like structure was predominant in the catalyst $[C\text{-}Zn]_{3,b}$. The graphitic structure was, however, considerably less in the catalyst $[C\text{-}ZnFe]_{2,b}$ and was finally diminished in the catalyst $[C\text{-}ZnFe]_{4,b}$. It was also observed that due to a very low iron content in the catalyst $[C\text{-}ZnFe]_{4,b}$, the XRD plots were unable to depict the *d* value and the size of the crystal for iron salt in this catalyst.

3.3. Thermogravimetric analysis

Thermogravimetric analysis of the catalyzed gasification of the CBCs in the presence of O_2 was conducted to obtain information about the extent of the activity of the catalysts [22,25]. The analysis consisted of heating the catalyst in an O_2 environment over a temperature range of 200–600°C and monitoring the weight loss of the CBCs as the oxidation reaction progressed. The TGA study was conducted using pure (99.99%) O_2 gas at a flow rate of 100 ml/min, and a heating rate of 5°C/min. The average particle size of the CBCs studied was 600 μm. Fig. 5 shows the extent of the catalytic gasification as a function of temperature. As shown, the weight loss or the amount of oxidation remains constant for the catalysts up to 300°C. The sharp increase in the weight loss at 300–500°C temperature was

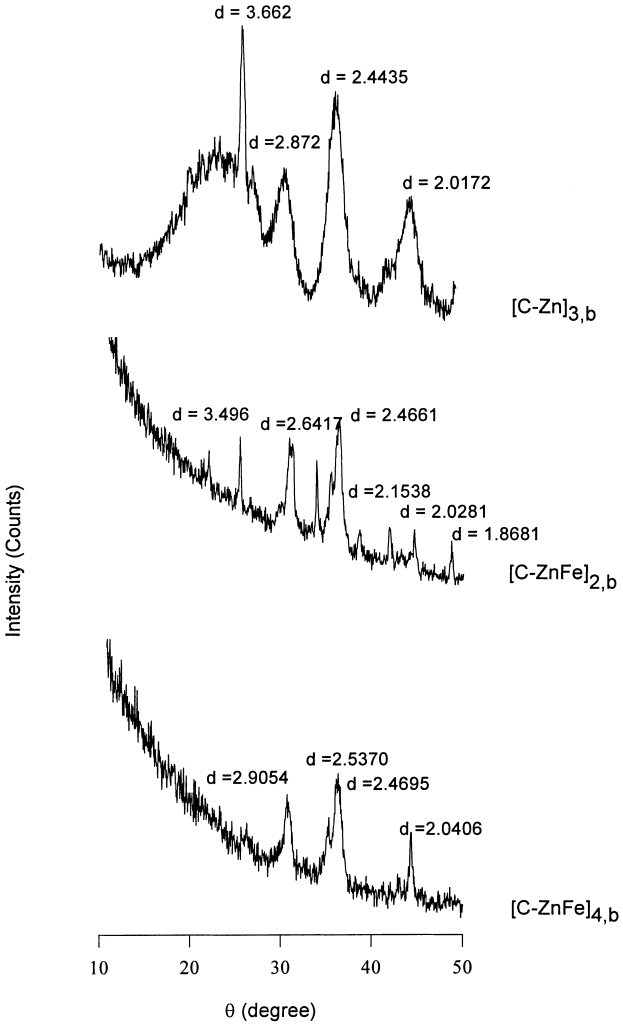

Fig. 4. X-ray diffraction of the produced CBCs.

related to the promotion of the pore diffusion and enhancement of the surface oxidation of unsaturated sites. The expected reaction at this temperature range is the formation of surface functional groups that subsequently decompose as CO_2 gas.

$$[\text{C-ZnFe}](s) + O_2(g) \rightarrow CO_2(g), \quad 300\text{–}500^{\circ}\text{C} \tag{3}$$

$$CO_2(g) + O_2(g) \rightarrow 2CO(g), \quad > 500^{\circ}\text{C} \tag{4}$$

The constant pattern observed above 500°C indicated that at temperatures >500°C, the CBCs are completely saturated with oxygen and further oxidation reaction results in the formation of a surface functional group that subsequently decomposes as CO gas [25].

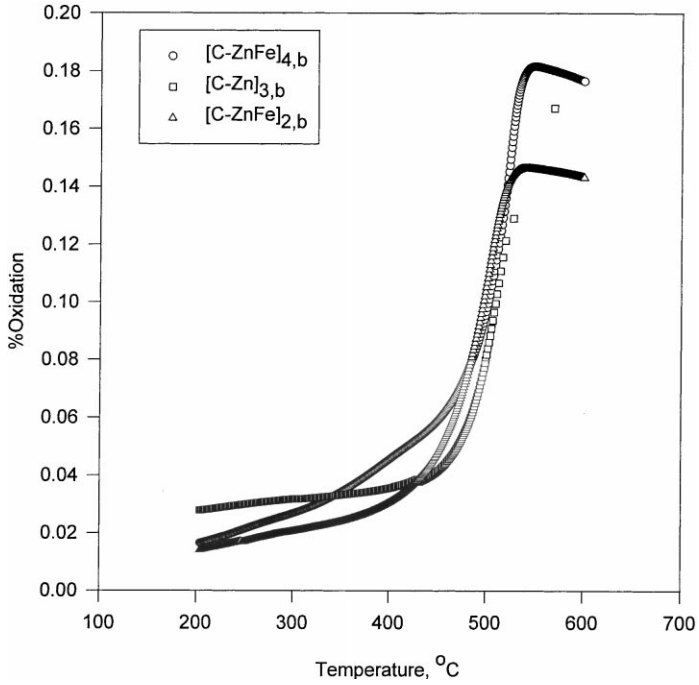

Fig. 5. Thermogravimetric analysis of the CBCs in O_2.

TGA data also suggested that due to the possible presence of unsaturated or active sites, at the temperature range of 400–450°C, catalysts $[C\text{-}ZnFe]_{2,b}$ and $[C\text{-}ZnFe]_{4,b}$ were oxidized to a greater extent than the catalyst $[C\text{-}Zn]_{3,b}$. The maximum amount of weight loss was observed for the catalyst $[C\text{-}ZnFe]_{4,b}$ at the temperature range of 400–500°C.

The surface oxidation reaction rate constants and the activation energy (E_0) associated with the catalyzed reactions carried out in the presence of oxygen were also evaluated from the TGA data assuming that $R \cong -(1/m_c)(dm_c/dt) \cong -(dC/dt) = KC$, and $K = K_0 \exp(-E_0/RT)$. The m_c, R, K and E_0 represented the mass of the catalyst at time t, the reaction rate, rate constant and the activation energy, respectively.

The estimated activation energy and the rate constant for the catalytic gasification reactions were 0.0886, 9.186, 2.672 kcal/mol K, and 3.89×10^{-4}, 3.33×10^{-2}, and 3.88×10^{-3}, for $[C\text{-}Zn]_{3,b}$, $[C\text{-}ZnFe]_{2,b}$, and $[C\text{-}ZnFe]_{4,b}$, respectively. The presence of iron and the enhanced process of iron oxide formation accounted for the increase in observed activation energy obtained for catalysts $[C\text{-}ZnFe]_{2,b}$ and $[C\text{-}ZnFe]_{4,b}$ (9.186 and 2.672 compare to 0.0886 for $[C\text{-}Zn]_{3,b}$).

3.4. NO_x reduction capability of the CBCs

3.4.1. Effect of catalyst surface structure

The characteristics of the catalytic NO_x removal were studied in a reduced environment (presence of CO gas), using a fixed bed reactor. The reaction temperature varied from

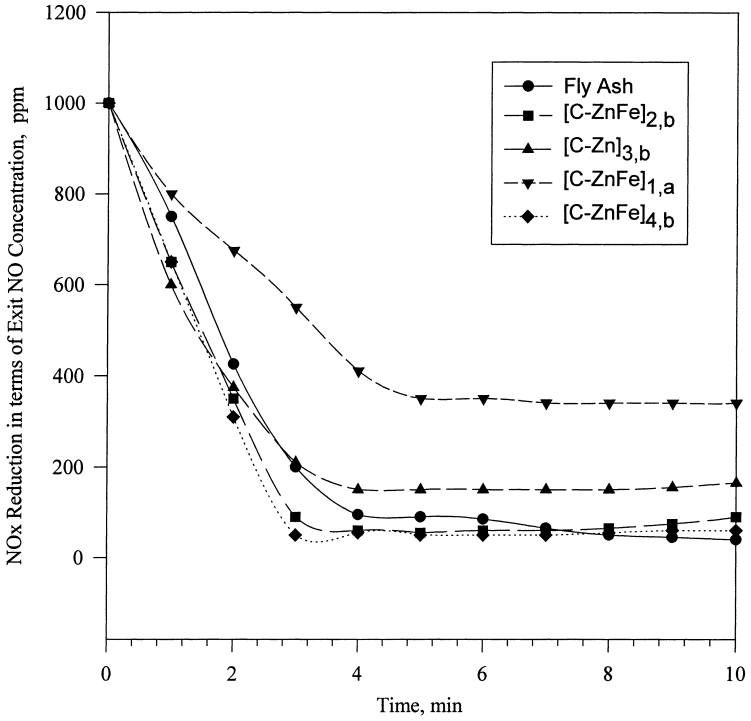

Fig. 6. Characteristics of catalytic NO_x reduction on CBCs ($T = 400^{\circ}C$).

300 to 500°C. As shown in Fig. 6, the extent and the rate of NO_x reduction are significantly influenced by the attributes of the catalysts. The NO_x removal efficiency of the $[C\text{-}ZnFe]_{1,a}$ catalyst was increased by 30% when post pyrolysis rinsing was used to synthesize $[C\text{-}ZnFe]_{2,b}$. It is also shown that time required by the catalyst $[C\text{-}ZnFe]_{2,b}$ to achieve a specified NO_x conversion is less than that required by the catalyst $[C\text{-}ZnFe]_{1,a}$.

The observed 83% conversion efficiency for catalyst $[C\text{-}Zn]_{3,b}$ was related to its high surface area, microporous structure, pore diffusion, and the promoted catalytic reaction between NO and CO in the pore structure.

The increased catalytic capacity of the [C-ZnFe] catalysts was mainly due to the presence of iron in the structure, enhanced surface mesoporousity and the characteristics of the PSD. The $[C\text{-}ZnFe]_{4,b}$ catalyst prepared with a Zn:Fe molar ratio of 1:0.5 had an NO_x removal capacity of 94%, close to that found for the fly ash catalyst used as control in this study.

These results were in a good agreement with previous studies [4,18,26,27] and showed that: the presence of the active metals and a uniform PSD provide large accessible sites for a better gas–solid contact and high catalytic activity; carbons that have higher meso- and macroporosity are more suitable for catalysis applications because of the greater access they provide to the reactants; and high surface area provides more access for the reactants and better catalytic removal. The differences observed between $[C\text{-}ZnFe]_{2,b}$, and $[C\text{-}ZnFe]_{4,b}$ catalytic behavior suggested that catalysts with smaller micropore size exhibit larger resis-

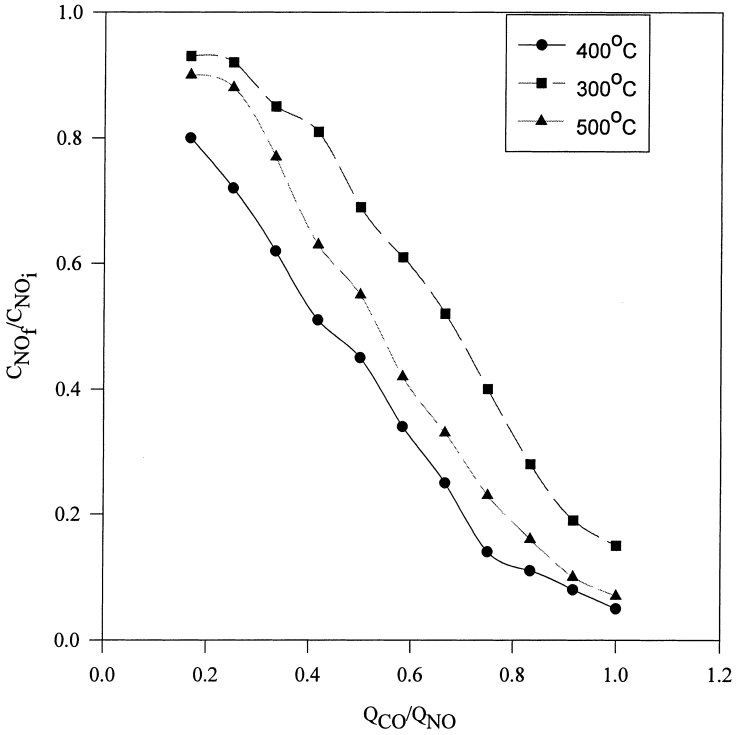

Fig. 7. Effect of CO flow rate and temperature on catalytic activity of $[C\text{-}ZnFe]_{4,b}$.

tance to the intra-particle diffusion, while mesoporous catalysts having a large amount of total surface area and a smaller micropore area can be very effective for NO_x reduction applications.

3.5. Effect of CO flow rate

The effect of the CO flow rate on the exit NO concentration (Q_{CO}) was tested to evaluate dependency of the catalyst activity on the amount of reducing agent used for catalysis. As shown in Fig. 7, the efficiency of the catalytic reaction decreased as the ratio of the CO to the NO flow rate increased. The minimum exit NO concentration was observed at $Q_{NO}/Q_{CO} = 1$, which is the stoichiometry of the catalytic reaction involved with complete reduction of NO to N_2:

$$CO + NO \rightarrow \tfrac{1}{2}N_2 + CO_2 \tag{5}$$

The lower conversion observed at $Q_{NO}/Q_{CO} < 1$ was related to the inhibition effect of a large amount of CO_2 generated at the enhancement surface oxidation process [5]. The low NO_x reduction efficiency observed at $Q_{NO}/Q_{CO} > 1$ was, however, affiliated with the absence of CO gas and incompleteness of the catalytic reactions.

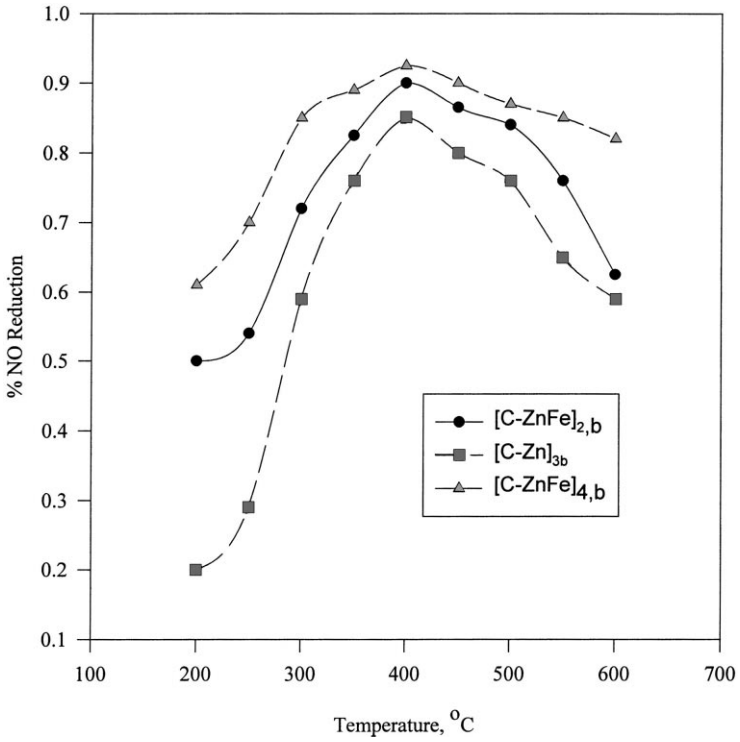

Fig. 8. Effect of temperature on catalytic activity of the produced CBCs.

3.6. Effect of temperature

Since it was shown that the catalytic activity of the $[C\text{-}ZnFe]_{4,b}$ is strongly dependent on the reaction temperature (Fig. 7); the produced CBCs were tested for their capability to reduce NO_x over a wide range of temperatures. As shown in Fig. 8, the maximum NO reduction efficiency obtained for the catalysts studied was at a reaction temperature of about 400°C.

The dependency of the catalytic reactions on temperature was explained by the fact that catalysis is a surface phenomenon, and adsorption of NO on the surface of the catalyst and reaction between the adsorbed NO and CO in the gas phase are temperature controlled process. Since at low temperature, molecular adsorption is the only expected surface phenomenon, NO preferentially reacts with CO in the gas phase and, therefore, surface catalytic reactions will be insignificant [6,8,12]. At $300^\circ C < T < 500^\circ C$, atomic adsorption process will be expected and as suggested by Gasser [8], in spite of the instability of the atomic layer, it covers the entire catalyst surface and promotes more interaction between the NO atom and active metal. The rapid adsorption of CO and promoted desorption of already adsorbed NO accounted for the observed low removal efficiencies at higher temperatures ($T > 500^\circ C$).

Table 2
Effect of method of production, and surface structure on the NO_x reduction efficiency of the produced CBCs

Catalyst	Zn:Fe molar ratio	Mesopore area (m^2/g)	NO_x conversion at 10 min (%)
Fly ash	NA	NA	96
$[C\text{-}ZnFe]_{1,a}$	1:1	205.16	66
$[C\text{-}ZnFe]_{2,b}$	1:1	226.65	90
$[C\text{-}Zn]_{3,b}$[a]	No iron	883.49	83
$[C\text{-}ZnFe]_{4,b}$	1:0.5	271.54	94

[a] Sample with zero iron.

Although, one can anticipate that mechanism of the reactions involved with the removal of NO_x on the surface of the produced CBCs are very complex, and therefore, it is difficult to draw any definite conclusion about the characteristic of the removal phenomena, it is very important to consider the fact that the NO removal activity strongly depends on the metal dispersion, carbon surface area, pore distribution, and synergic between C, Fe and Zn.

4. Conclusion

A series of CBCs were produced from paper mill sludge using zinc chloride and iron nitrate as impregnating agents. The customized method of production resulted in the synthesis of CBCs with high surface area, mesoporous structure, uniform PSD and high catalytic activity for reduction of NO_x in the flue gas. The method of production, surface properties (surface area, micro- and mesoporosity, PSD) and reaction temperature had a significant impact on the performance of the produced CBCs as a catalyst for NO_x removal (Table 2).

The maximum catalytic efficiency of 94% was obtained for the mesoporous catalyst ($[C\text{-}ZnFe]_{4,b}$) prepared at Zn:Fe molar ratio of 1:0.5. This catalyst had a surface area of 310 m^2/g, prominent mesoporosity and a uniform PSD. The optimum reaction temperature for the catalytic reduction was found to be 400°C.

The developed process is a high return/low risk method of waste reduction and recycling. The negative cost of the raw material, elimination of the need for the land disposal of sludge, and high potentials for producing a highly active catalysts, have signified the need for expanding the scope of this project. Work is in progress to evaluate the extent of the catalyst life, impact of the presence of other pollutants in the gas streams (i.e. water, oxygen, SO_2), effect of regeneration on the catalyst activity, and catalyst potentials for other air and water pollution applications such as removal of SO_2, mercury and H_2S from emission streams.

Acknowledgements

The authors would like to thank Dr. Giselle Sandi for supervising TGA and XRD experiments conducted at Argonne National Laboratory.

References

[1] United States Environmental Protection Agency (USEPA), Air Pollution Control Technology Seminar, Interagency Energy/Environment R&D Report, EPA-600/7-79-011, 1981, pp. 2.1–2.14.
[2] T. Grzybek, H. Papp, J. Appl. Catal. B 1 (1992) 271–283.
[3] T. McQueen, in: Proceedings of the 35th IEEE Cement Industry Technical Conference, Toronto, Canada, May 23–27, 1993, 241 pp.
[4] J.K. Neathery, A.M. Rubel, J.M. Stencel, J. Carbon 35 (35) (1997) 1321–1327.
[5] S. Stegenga, R. Van Soest, F. Kapteijn, J.A. Moulijn, J. Appl. Catal. B: Environ. 2 (2) (1993) 257–275.
[6] S. Shen, H. Weng, J. Ind. Eng. Chem. Res. 37 (1998) 2654–2661.
[7] M. Beaupre, S. Macdonnell, M. Nisbet, Proceedings of the 30th International Cement Seminar, Sponserved by Rock Products, Chicago, IL, 1994, pp. 139–146.
[8] R.P.H. Gasser, in: An Introduction to Chemisorption and Catalysis by Metals, Clarendon Press, Oxford, 1985, pp. 211–223.
[9] H. Randall, R. Doepper, A. Renken, J. Appl. Catal. B: Environ. 17 (1998) 357–369.
[10] C. Martinery, M. Vannice, J. Carbon 28 (4) (1990) 467–476.
[11] G.Q.(Max) Lu, J. Environ. Prog. 15 (1) (1996) 12–18.
[12] I. Mochida, S. Kisamori, M. Hironaka, S. Kawano, Y. Matsumura, M. Yoshikawa, J. Energy Fuels 8 (1994) 1341–1344.
[13] E. Ruckenstein, Y.H. Hu, J. Ind. Eng. Chem. Res. 36 (1997) 2533–2536.
[14] A.A. Lizzio, J.A. DeBarr, J. Energy Fuels 11 (1997) 284–291.
[15] G.Q. Lu, D.D. Do, J. Carbon 29 (2) (1991) 207–213.
[16] N.R. Khalili, H. Arastoopour, L.K. Walhuf, IIT Patent No. 6030922.
[17] F. Rodriguez-Reinoso, M. Molina-Sabio, J. Adv. Colloid Interface Sci. 76/77 (1998) 271–294.
[18] S. Boppart, L. Ingle, R.J. Potwora, D.O. Rester, J. Chem. Process. 79 (1996) 79–84.
[19] J.V. Ibbarra, J. Fuel 70 (1991) 727–732.
[20] L.K. Walhof, Procedure to Produce Activated Carbon from Biosolids, Master's Thesis, IIT-CHEE, 1998, pp. 20–50.
[21] S.R. Dhakate, R.B. Mathur, O.P. Bahl, J. Carbon 35 (12) (1997) 1753–1756.
[22] S.J. Gregg, K.S.W. Sing, Adsorption, Surface Area, and Porosity, 2nd Edition, Academic Press, London, 1982, pp. 100–125.
[23] B.D. Cullity, Elements of X-ray Diffraction, Addison-Wesley, Reading, MA, 1956.
[24] N.R. Khalili, M. Pan, G. Sandi, J. Carbon 38 (4) (2000) 573–588.
[25] J.S. Mattson, B.H. Mark, Surface Chemistry and Adsorption from Solution, Marcel Dekker, New York, 1971.
[26] S. Mikhalovsky, Yu.P. Zaitsev, J. Carbon 35 (9) (1997) 1367–1374.
[27] P. Davini, J. Carbon 31 (1) (1993) 147–151.